J|A|C|S
ARTICLES

Published on Web 03/24/2009

A Sulfur-Terminal Zn(II) Complex and Its Two-Photon Microscopy Biological Imaging Application

Yuanhao Gao,[†] Jieying Wu,[†] Yiming Li,[‡] Pingping Sun,[†] Hongping Zhou,[†] Jiaxiang Yang,[†] Shengyi Zhang,[†] Baokang Jin,[†] and Yupeng Tian*[,†,§,⊥]

Department of Chemistry, Key Laboratory of Inorganic Materials Chemistry of Anhui Province, Anhui University, Hefei 230039, P.R. China, State Key Laboratory of Crystal Materials, Shandong University, Jinan 250100, P.R. China, State Key Laboratory of Coordination Chemistry, Nanjing University, Nanjing 210093, P.R. China, and Department of Chemistry, University of Science and Technology of China, Hefei 230026, P.R. China

Received November 10, 2008; E-mail: yptian@ahu.edu.cn

Abstract: A novel sulfur-terminal Zn(II) complex $Zn(S)_2L$ (L = *N*-hexyl-3-{2-[4-(2,2′:6′,2″-terpyridin-4′-yl)phenyl] ethenyl}carbazole) was obtained by a facile solvothermal process. The unique feature in this new reaction design is the use of ZnS nanocrystals as a precursor and bulky chromophoric L as an ancillary ligand. The versatility of the two terminal sulfur atoms is relevant to biological system. The resulting $Zn(S)_2L$ complex shows two-photon excited fluorescence (TPEF), which has been proven to be potentially useful for two-photon microscopy imaging in living cells. In addition, cytotoxicity tests showed that the low-micromolar concentrations of $Zn(S)_2L$ did not cause significant reduction in cell viability over a period of at least 24 h and should be safe for further biological studies.

Introduction

Transition metal−sulfur chemistry is of immense biological importance.[1−4] Many important metal−sulfur enzymes and electron transfer proteins incorporate a wide range of metals (V, Fe, Ni, Cu, Zn, Mo, and W) and sulfur-containing ligands or moieties, which have attracted considerable attention in the synthesis and structural investigations of transition metal sulfide or sulfur-containing complexes.[5−11] Due to the strong covalent nature between sulfur and transition metal (caused by the strong π-donation from sulfur to metal center),[12,13] the sulfur atoms often bridge metal centers to form various metal sulfide clusters.

Scheme 1. Molecular Structure of L

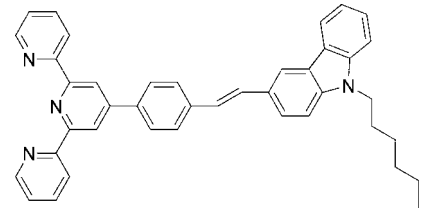

So far, there are few demonstrations of sulfur-terminal complexes,[14−16] though the structural type is highly desirable because of the versatility of terminal sulfur (such as second coordination, S···H bonding, and pH sensitivity) and its relevance to the biological system. Therefore, it remains challenging to develop a rational method to construct the transition metal complex with a sulfur atom as a terminal ligand.

We have devoted considerable effort to address this problem. It was found that a bulky ancillary organic ligand and inorganic nanocrystals (transition metal sulfide) as precursors are favorable for the formation of sulfur-terminal mononuclear complex. This is most likely due to the following two facts: (i) the inorganic nanocrystals (transition metal sulfide) could provide both a metal source and sulfur source immediately, and it may avoid the potential side effect of other ions; (ii) the large steric bulkiness of the organic ligand competes with the bridging tendency of sulfur atoms and, thus, results in a mononuclear complex with sulfur atoms as terminal ligands.

[†] Anhui University.
[‡] University of Science and Technology of China.
[§] Shandong University.
[⊥] Nanjing University.

(1) Stiefel, E. I., Matsumoto, K., Eds. *Transition Metal Sulfur Chemistry: Biological and Industrial Significance*; ACS Symposium Series 653, American Chemical Society: Washington, DC, 1996.
(2) Holm, R. H.; Kennepohl, P.; Solomon, E. I. *Chem. Rev.* **1996**, *96*, 2239–2314.
(3) Articles in the Bioinorganic Enzymology thematic issue: *Chem. Rev.* **1996**, *96*, 2315−3042.
(4) Bertini, I.; Gray, H. B.; Stiefel, E. I.; Valentine, J. S. *Biological Inorganic Chemistry: Structure and Reactivity*; University Science Books: Sausalito, CA, 2007.
(5) Matsumoto, K.; Yoichi Sano, Y. *Inorg. Chem.* **1997**, *36*, 4405–4407.
(6) Li, Z.; Du, S.; Wu, X. *Inorg. Chem.* **2004**, *43*, 4776–4777.
(7) Kuckmann, T. I.; Hermsen, M.; Bolte, M.; Wagner, M.; Lerner, H. W. *Inorg. Chem.* **2005**, *44*, 3449–3458.
(8) Zhang, Y.; Zuo, J. L.; Zhou, H. C.; Holm, R. H. *J. Am. Chem. Soc.* **2002**, *124*, 14292–14293.
(9) Hossain, Md. M.; Lin, H. M.; Shyu, S. G. *Organometallics* **2004**, *23*, 3941–3949.
(10) Henkel, G.; Krebs, B. *Chem. Rev.* **2004**, *104*, 801–824.
(11) Adams, R. D.; Captain, B.; Kwon, O.-S.; Miao, S. *Inorg. Chem.* **2003**, *42*, 3356–3365.
(12) Amerasekera, J.; Rauchfuss, T. B.; Wilson, S. R. *Inorg. Chem.* **1987**, *26*, 3328–3332.
(13) Matsumoto, K.; Matsumoto, T.; Kawano, M.; Ohnuki, H.; Shichi, Y.; Nishide, T.; Sato, T. *J. Am. Chem. Soc.* **1996**, *118*, 3597–3609.
(14) Eagle, A. A.; Gable, R. W.; Thomas, S.; Sproules, S. A.; Young, C. G. *Polyhedron* **2004**, *23*, 385–394.
(15) Doonan, C. J.; Nielsen, D. J.; Smith, P. D.; White, J. M.; George, G. N.; Young, C. G. *J. Am. Chem. Soc.* **2006**, *128*, 305–316.
(16) Young, C. G. *J. Inorg. Biochem.* **2007**, *101*, 1562–1585.

10.1021/ja808606d CCC: $40.75

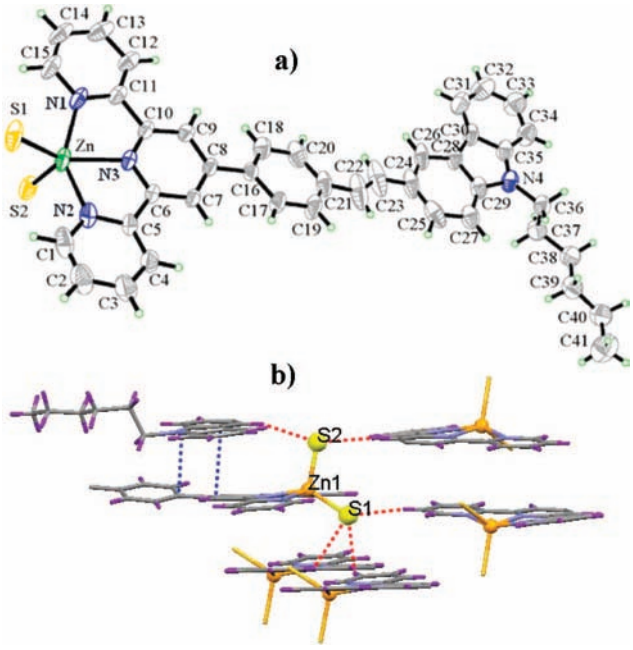

Figure 1. (a) Crystal structure of $Zn(S)_2L$ showing 50% probability displacement. (b) Intermolecular S···H hydrogen bondings (red lines) and $\pi\cdots\pi$ interactions (blue lines) in crystal packing of $Zn(S)_2L$.

We are primarily interested in the d-block metal Zn(II), a functional metal ion in almost 300 enzymes.[17,18] In this work, we utilized a facile solvothermal reaction process toward the target Zn(II) complex. ZnS nanocrystals were used as both a zinc source and sulfur source. The selected bulky organic ligand was *N*-hexyl-3-{2-(4-(2,2′:6′,2″-terpyridin-4′-yl)phenyl)ethenyl}-carbazole (labeled as L in Scheme 1). The bulky L is a highly π-conjugated chromophore, which contains a terpyridinyl tridentate chelate group,[19] a two-photon active carbazole moiety,[20] a flexible hexyl chain, and a phenylethenyl group as a π-conjugated bridge. The complex $Zn(S)_2L$ was obtained in high yield without any other counterions (see Figure 1a). Significantly, the two sulfur atoms in the complex are identical in the minus one oxidation state (S^{1-}) and coordinated to Zn(II) as terminal ligands, which is unknown previously in a Zn(II) complex. The structure of the complex has been studied by X-ray single crystal analysis and DFT calculation in this work.

On the other hand, since Zn(II) has a closed-shell d^{10} electronic configuration, it was anticipated that its coordination with the chromophore L would produce fluorescence characteristics dependent on the L ligand.[21] In the course of investigating the optical properties of the $Zn(S)_2L$ complex, we discovered it had interesting two-photon excited fluorescence, which should be potentially useful for two-photon microscopy imaging. Two-photon microscopy offers a number of advantages in biological imaging, including reduced phototoxicity, increased penetration depth, and negligible background fluorescence, and thus it has now become the primary fluorescence imaging technique.[22,23] With the above consideration, we further explored the application of the two-photon excitation properties of $Zn(S)_2L$ for two-photon imaging in living cells. The results showed that the $Zn(S)_2L$ complex is cell-permeable and suitable for cytoplasm staining and uptake. Cytotoxicity tests indicated that the sub- and low-micromolar concentrations of $Zn(S)_2L$ are essentially nontoxic. The novel structural mode of the $Zn(S)_2L$ complex and its application for *in vivo* two-photon imaging make it intrinsically interesting at least to bioinorganic chemists for further biological studies.

Results and Discussion

Synthesis of $Zn(S)_2L$ Complex. The complex $Zn(S)_2L$ was obtained as red single crystals ($1.2 \times 1.0 \times 1.1$ mm^3) by treating the mixture of pure ZnS nanocrystals, ligand L, and NaSCN in ethanol in a solvothermal process. The ZnS nanocrystals used as precursor are the zinc blende phase of ZnS with an average diameter of 9.0 nm, which were synthesized by the reaction of $Zn(CH_3COO)_2\cdot 2H_2O$ and CH_3CSNH_2 in ethanol at 80 °C. Here, NaSCN is used as a mineralizer to improve the single crystal quality. To obtain the big cubic block crystals, it is needed to control the content of NaSCN in the range 0.2−0.5 equiv in the synthetic condition. Without the presence of NaSCN, only the small red crystallites of $Zn(S)_2L$ turned up. We have also attempted to react the mixture of $Zn(CH_3COO)_2\cdot 2H_2O$, CH_3CSNH_2, ligand L, and NaSCN in one pot in the solvothermal process. But no single crystal suitable for X-ray analysis was yielded; only unidentified red precipitates were observed. This result indicates that the pure ZnS nanocrystals may be the optimal precursor, which can simultaneously provide both the zinc source and sulfur source in the production of the sulfur-terminal Zn(II) complex.

Structure Investigation of $Zn(S)_2L$ Complex. The structure of the $Zn(S)_2L$ complex was confirmed by X-ray crystallography. In the complex (Figure 1a), the Zn(II) center is in a distorted 5-coordinated trigonal-bipyramidal geometry with the two apical sites occupied by two sulfur atoms. The S1−Zn−S2 bond angle is 110.46(5)°. The equatorial plane is comprised of the three N atoms (N1, N2, and N3) of ligand L, and the distance between Zn(II) center and the equatorial plane is 0.340 Å. The N−Zn bond lengths are 2.188(3) Å for N1−Zn, 2.096(2) Å for N2−Zn, and 2.200(3) Å for N3−Zn, which are within the normal range.[24−26] To be emphasized, the S−Zn bond lengths are 2.2565(11) Å for S1−Zn and 2.2600(11) Å for S2−Zn, which are significantly shorter than that in previous literatures, even are evidently short relative to that in the ZnS crystal lattice (2.35 Å for zinc blende ZnS; 2.36 Å for wurtzite ZnS). The S−Zn bond length data indicate there is a strong covalent nature between sulfur atoms and the zinc(II) center.

Interestingly, it can be seen that $Zn(S)_2L$ is an overall neutral complex, without any other counterions. The fact that the two S−Zn bond lengths are almost equal (2.2565 versus 2.2600 Å) suggests that both sulfur atoms should be in the same oxidation state in the Zn(II) complex and excludes the possibility that the one sulfur atom is S^0 and the other is S^{2-}. Two S^{2-} valence states are also excluded since it would result in the formation of an unlikely Zn(IV) complex. As a result, sulfur atoms are

(17) Vahrenkamp, H. *Acc. Chem. Res.* **1999**, *32*, 589–596.
(18) Peariso, K.; Goulding, C. W.; Huang, S.; Matthews, R. G.; Penner-Hahn, J. E. *J. Am. Chem. Soc.* **1998**, *120*, 8410–8416.
(19) Constable, E. C. *Chem. Soc. Rev.* **2007**, *36*, 246–253.
(20) Shirota, Y.; Kageyama, H. *Chem. Rev.* **2007**, *107*, 953–1010.
(21) Nolan, E. M.; Lippard, S. J. *Acc. Chem. Res.* **2009**, *42*, 193–203.
(22) Larson, D. R.; Zipfel, W. R.; Williams, R. M.; Clark, S. W.; Bruchez, M. P.; Wise, F. W.; Webb, W. W. *Science* **2003**, *300*, 1434–1436.
(23) Kim, H. M.; Jeong, B. H.; Hyon, J. Y.; An, M. J.; Seo, M. S.; Hong, J. H.; Lee, K. J.; Kim, C. H.; Joo, T.; Hong, S. C.; Cho, B. R. *J. Am. Chem. Soc.* **2008**, *130*, 4246–4247.
(24) Schmittel, M.; Kalsani, V.; Kishore, R. S. K.; Colfen, H.; Bats, J. W. *J. Am. Chem. Soc.* **2005**, *127*, 11544–11545.
(25) Nicholson, G. A.; Petersen, J. L.; McCormick, B. J. *Inorg. Chem.* **1982**, *21*, 3274–3280.
(26) Einstein, F. W. B.; Penfold, B. R. *Acta Crystallogr.* **1966**, *20*, 924–926.

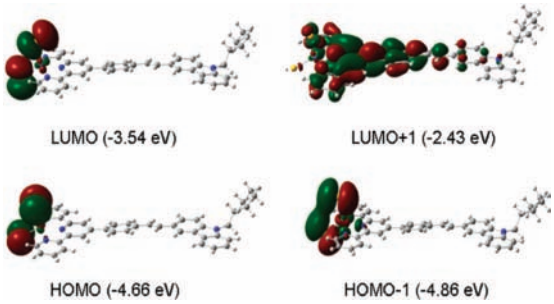

Figure 2. Representation of calculated Kohn−Sham orbitals of complex $Zn(S)_2L$.

most likely to be two identical S^{1-} valence states, unknown previously in a Zn(II) complex. The two identical S^{1-} valence states could be a result of charge self-regulation in this complex due to the orbital hybridization of S1−Zn−S2 since there is a strong covalent nature between sulfur atoms and the zinc metal center. Charge self-regulation behavior have been observed in transition metal complexes and proven to be the result of orbital hybridization, electron delocalization, and resonance, which were reported recently.[27,28] To better understand the two sulfur oxidation states, density functional theory (DFT) calculations on $Zn(S)_2L$ were carried out. The molecular geometry used for the calculation is obtained from X-ray diffraction crystallographic data.

Figure 2 gives straightforward representations of the electron density distribution. The calculated results show that the electron density distributions in the two sulfur atoms are very similar. Orbital analysis exhibits that the highest occupied molecular orbital (HOMO) is comprised of sulfur atom π character with a smaller contribution from Zn d_{xz}. Also the lowest unoccupied molecular orbital (LUMO) distribution is localized in the sulfur π orbitals with minor Zn d_{yz}. Hereby, there are relatively strong π-donor interactions between sulfur atoms and the zinc center, and the electron density in each sulfur atom is very similar. It is most likely that there is an electron resonance structure of S1−Zn−S2 with the sulfur electron resonance of $S^0 \leftrightarrow S^{1-} \leftrightarrow S^{2-}$, resulting in two identical S^{1-} valence states. Here, the Zn(II) center should adopt sp^3d hybridized orbitals, which is common in a 5-coordinated Zn(II) complex. In nature, a S1−Zn−S2 bond angle of 110.46(5)° is within the range of 100°−120° reported and is feasible for their orbital hybridization, electron delocalization, and resonance.[2,29] Thus, the two S^{1-} valence states are reasonably explained to the overall neutral Zn(II) complex and the two equal S−Zn bond lengths.

Note alo the multiple S···H hydrogen bonds in the crystal packing of $Zn(S)_2L$ (Figure 1b). There are three S···H bondings to the S1 atom and two S···H bondings to the S2 atom, which are listed in Table 1. The multiple S···H hydrogen bonds arise from the nature of the unsaturated coordination of sulfur atoms. In crystal packing, the multiple S···H bonds and prolific intermolecular π...π interactions stabilize these $Zn(S)_2L$ molecules in a 3D supramolecular configuration (Figure S3). The multiple S···H bonds suggest the versatility of the structural type and its relevance to biological systems.

Linear Absorption and Single-Photon Excited Fluorescence (SPEF) of $Zn(S)_2L$. As shown in Figure 2, on the LUMO+1 molecular orbital, the electrons delocalize over the L ligand,

Table 1. Intermolecular C−H···S Hydrogen Bondings in $Zn(S)_2L$ Crystal

C−H···S	C−H/Å	C···S/Å	H···S/Å	∠C−H···S /°
C14−H14···S1	0.930	3.563	2.693	172.66
C2−H2···S1	0.930	3.544	2.980	120.57
C12−H12···S1	0.929	3.601	2.985	125.13
C26−H26···S2	0.930	3.787	2.897	160.81
C4−H4···S2	0.930	3.686	2.771	168.21

which reveals that $Zn(S)_2L$ could yield the desired photophysical properties (absorption and fluorescence) dependent on the L ligand. Figure 3 shows the UV−vis absorption spectra of the complex $Zn(S)_2L$ and pure L. The free L showed its two characteristic absorption bands centered at 283 and 360 nm (Figure 3a) while the two absorption bands in the complex $Zn(S)_2L$ red-shifted to 299 and 406 nm, respectively, *via* coordination between the L and zinc center (Figure 3b). A new band at 326 nm observed in the absorption spectra is probably due to the interaction between zinc(II) and sulfur (S^{1-}) in the complex (Figure 3b). Figure 4 shows the single-photon excited fluorescence (SPEF) spectrum of the $Zn(S)_2L$ complex in DMF. A broad emission band centered at 525 was observed, which is a contribution from the L ligand. The fluorescence lifetime (τ) was 1.62 ns in DMF (Figure S5). The fluorescence quantum efficiency (Φ) was 0.31, which was determined by using Coumarin 307 as the standard.

Two-Photon Excited Fluorescence (TPEF) of $Zn(S)_2L$. It was found that there was no linear absorption in the wavelength

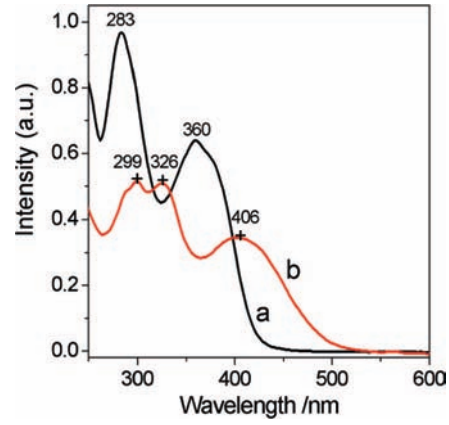

Figure 3. UV−vis absorption spectra of (a) pure L and (b) $Zn(S)_2L$ in DMF at an identical concentration of 1.0×10^{-5} mol·L^{-1}.

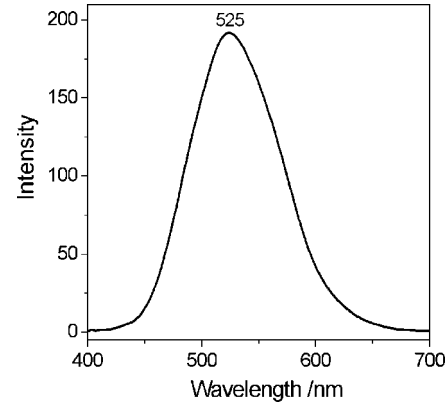

Figure 4. Single-photon excited fluorescence (SPEF) spectrum of $Zn(S)_2L$ in DMF (1.0×10^{-6} mol·L^{-1}) with excitation wavelength at 400 nm.

(27) Raebiger, H.; Lany, S.gl594; Zunger, A. *Nature (London)* **2008**, *453*, 763–766.
(28) Resta, R. *Nature (London)* **2008**, *453*, 735–735.
(29) Chakrabarti, P. *Biochemistry* **1989**, *28*, 6081–6085.

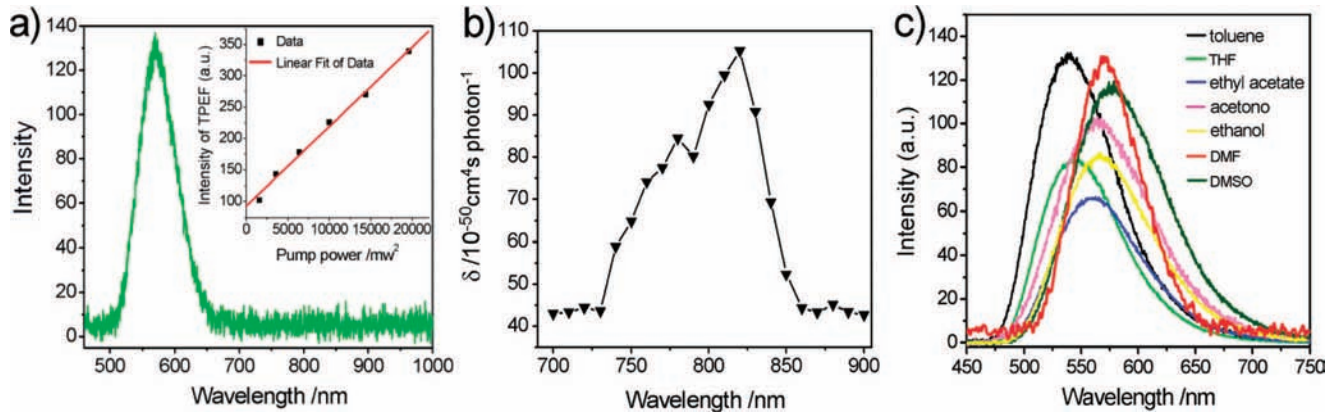

Figure 5. Two-photon action: (a) Two-photon excited fluorescence (TPEF) spectrum of $Zn(S)_2L$ in DMF ($C = 1.0 \times 10^{-3}$ mol L^{-1}) at the optimal excitation wavelength of 820 nm. Inset: Fluorescence power dependence, excitation carried out at 800 nm. (b) Two-photon (200 fs, 76 MHz Ti:sapphire laser) absorption cross section of $Zn(S)_2L$ in DMF versus excitation wavelengths of identical energy of 0.380 w. (c) Two-photon excited fluorescence (TPEF) spectrum of $Zn(S)_2L$ in seven solvents of differing polarity ($C = 1.0 \times 10^{-3}$ mol L^{-1}).

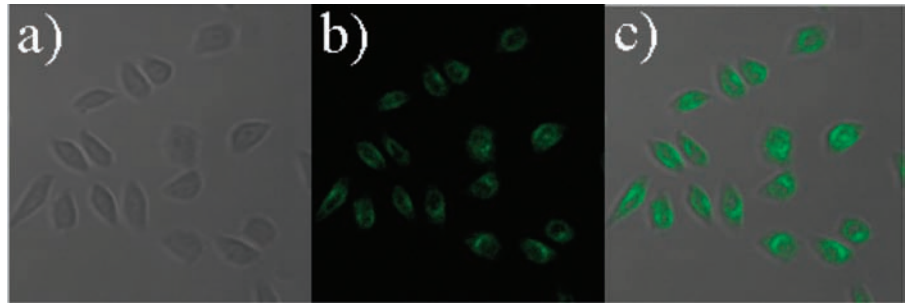

Figure 6. (a) Bright-field image of the HeLa cells stained with $Zn(S)_2L$. (b) Two-photon microscopy (TPM) image of the same cells with excitation at 800 nm. (c) Merged image.

range 700−900 nm for the $Zn(S)_2L$ complex, which indicates that there are no energy levels corresponding to an electron transition in the spectral range. Therefore, upon excitation from 700 to 900 nm, it is impossible to produce single-photon-excited up-converted fluorescence. If frequency upconverted fluorescence occurs upon excitation with a tunable laser in the range 700−900 nm, it can be safely attributed to multiphoton excited fluorescence. In our measurements, the $Zn(S)_2L$ complex presented a bright two-photon excited fluorescence (TPEF) centered at 570 nm in DMF with an optimal excitation wavelength of 820 nm (Figure 5a). As shown in the inset in Figure 5a, the emission intensities of the $Zn(S)_2L$ complex were investigated at 800 nm. The linear dependence of output fluorescence intensity (I_{out}) on the square of input laser power (mw^2) confirms that this is a two-photon excitation mechanism. The two-photon absorption (TPA) spectra of the $Zn(S)_2L$ complex were determined in the wavelength range 700−900 nm in DMF (1.0×10^{-3} mol L^{-1}) by the two-photon-induced fluorescence method with fluorescein as the standard.[30,31] The details are given in the Experimental Section. The experiments were conducted in the femtosecond regime, thereby preventing contribution from linear nonresonant absorption or from excited-state absorption. These are known to cause artificially enhanced "effective" TPA cross sections if measurements were conducted in the nanosecond regime. Detailed experiments reveal that the peak position of the TPEF spectra of the $Zn(S)_2L$ complex are independent of the excitation wavelengths (from 700 to 900 nm), but the two-photon absorption cross sections (δ) are dependent over that range. By tuning the pump wavelengths incrementally from 700 to 900 nm while keeping the input power constant and then recording the TPEF intensity, the two-photon absorption spectra of the $Zn(S)_2L$ complex are obtained (see Figure 5b). The spectra display one excitation peak and is similar to that observed in the linear absorption spectra, except that the wavelengths are roughly doubled. In the measured range, the maximal TPA cross section (δ) is 105.2 GM (1 GM = 10^{-50} cm^4 s $photon^{-1}$) at 820 nm. It is worth underlining that this value exceeds that of many fluorophores widely used in biology, including fluorescein, BODIPY, DAPI, GFP, or other complexes.[31−34] Furthermore, the two-photon excited fluorescence of the $Zn(S)_2L$ complex depends on the solvent polarity. Figure 5c shows the two-photon excited fluorescence spectra in seven common solvents of differing polarity. All spectra exhibited a broad emission band, and the emission maximum shifted to a longer wavelength with the increase of the solvent's polarity.

Two-Photon Microscopy Biological Imaging Application of $Zn(S)_2L$. To demonstrate the potential applications of $Zn(S)_2L$ for two-photon microscopy (TPM) imaging in living cells, HeLa cells were cultured and stained with $Zn(S)_2L$. A bright-field image (Figure 6a) of each cell was taken immediately prior to the two-photon microscopy (TPM) imaging. The TPM image and the merged image confirm that the molecules of $Zn(S)_2L$ are presented within the cells (Figure 6b,c). Herein, the cytoplasmic distribution is more uniform, and the distribution

(30) Lee, S. K.; Yang, W. J.; Choi, J. J.; Kim, C. H.; Jeon, S.-J.; Cho, B. R. *Org. Lett.* **2005**, *7*, 323–326.
(31) Xu, C.; Webb, W. W. *J. Opt. Soc. Am. B* **1996**, *13*, 481–491.
(32) Xu, C.; Zipfel, W.; Shear, J. B.; Williams, R. M.; Webb, W. W. *Proc. Natl. Acad. Sci. U.S.A.* **1996**, *93*, 10763–10768.
(33) Picot, A.; Malvolti, F.; Le Guennic, B.; Baldeck, P. L.; Williams, J. A. G.; Andraud, C.; Maury, O. *Inorg. Chem.* **2007**, *46*, 2659–2665.
(34) Picot, A.; D'Aléo, A.; Baldeck, P. L.; Grichine, A.; Duperray, A.; Andraud, C.; Maury, O. *J. Am. Chem. Soc.* **2008**, *130*, 1532–1533.

Table 2. Cytotoxicity Data (HeLa, 24 h)[a]

$Zn(S)_2L$ concentration	2 μM	5 μM	10 μM	20 μM
% cell survival	94 ± 3	89 ± 6	56 ± 5	48 ± 1

[a] Cell viability was quantified by the MTT assay (mean ± SD).

in the nucleolus is significantly lower. Note the pure L does not permeate the cultured cells and only weak fluorescence is detected on the surface of cells. This result demonstrates that the observed cytoplasm uptake must be due to the presence of the intact $Zn(S)_2L$ complex. It was realized that the structure of the $Zn(S)_2L$ complex is similar to those of a series of zinc(II) bis(thiosemicarbazone) complexes,[35] which might imply that they have the same cell uptake mechanism, i.e., a protonation enhanced trapping process.[35] From the acridine orange staining experiments and the cell uptake of zinc(II) bis(thiosemicarbazone) complexes, it was confirmed that these bright sites are lysosomes which have a lower pH in the system. The unsaturated coordination of the two sulfur atoms in $Zn(S)_2L$ are assumed to be pH-sensitive in the biologically relevant pH range and thus to be readily protonated in these lysosomes, which is most probably responsible for the intracellular localization of the $Zn(S)_2L$ complex. The multiple S···H bonds observed in the solid state structure indicate that such interactions are feasible (the shortest S···H bond length is 2.639 Å) (see Table 1).

Cytotoxicity is a potential side effect of $Zn(S)_2L$ that must be controlled when dealing with living cells or tissues. To this end, we have conducted cytotoxicity assays in HeLa cells. Table 2 lists the cell viability data for HeLa cells treated with $Zn(S)_2L$ as quantified by the MTT assay, an established method of probing cell death. These data show that HeLa cells show nearly ~100% viability following 24 h of treatment with 2 μM $Zn(S)_2L$. Higher concentrations result in decreased cell survival, with 56% and 48% viability observed following 24 h of treatment with 10 and 20 μM $Zn(S)_2L$. These cytotoxicity tests show that sub- and low-micromolar concentrations of $Zn(S)_2L$ are essentially nontoxic over a period of at least 24 h and could safely be used for further biological studies.

Conclusion

In conclusion, the first sulfur-terminal zinc-coordination complex $Zn(S)_2L$ with two-photon excited fluorescence has been obtained by a facile solvothermal process. The unique feature in this new reaction design is the use of ZnS nanocrystals as a precursor and chromophoric L as an ancillary ligand. It is observed that the $Zn(S)_2L$ complex is of sufficient stability and biological relevance. The novel structural mode of the $Zn(S)_2L$ complex and its two-photon excited fluorescence imaging should be intrinsically interesting to chemists, biologists, and material scientists. Particularly, the versatility of the two unsaturated coordinated sulfur atoms could be expected to endow $Zn(S)_2L$ significant promise not only for biomedical applications but also as a "complex" ligand for the surface modification of nanomaterials, even for the synthesis of novel hetero metal complexes.

Experimental Section

All chemicals were commercially available and used as obtained. The solvents were purified by conventional methods before use. Synthesis of *N*-hexyl-3-{2-(4-(2,2′:6′,2″-terpyridin-4′-yl)phenyl) ethenyl}carbazole (L) is available in the Supporting Information. ^{1}H NMR spectra were recorded with a Bruker AV400 NMR spectrometer. Elemental analyses were performed with a Perkin-Elmer 240B instrument. Fourier transform infrared (FT-IR) spectra were recorded on a SHIMADZU IR Prestige-21 spectrophotometer with samples prepared as KBr pellets. Ultraviolet−visible (UV−vis) absorption spectra were obtained with a SHIMADZU UV-3600 UV−vis−NIR spectrophotometer. X-ray power diffraction (XRD) measurements were performed on a Japan Rigaku DMax-γA rotation anode X-ray diffractometer equipped with graphite monochromatized Cu Kα radiation (λ = 1.541 78 Å).

Synthesis of ZnS Nanocrystals. In a typical procedure, $Zn(CH_3COO)_2 \cdot 2H_2O$ (219.5 mg, 1.0 mmol) and CH_3CSNH_2 (82.5 mg, 1.1 mmol) were dissolved in 50 mL of ethanol to form a transparent solution. Then the clear solution was refluxed at 80 °C with vigorous stirring for 3 h. The solution was changed gradually from a clear to white turbid solution. Finally, the white powders of ZnS nanocrystals were obtained by the subsequent centrifugation of the precipitates followed by washing several times with water and ethanol. The obtained ZnS nanocrystals (87.3 mg, 90% yields) are the zinc blende phase of ZnS with an average diameter of 9.0 nm (determined by XRD).

Synthesis of $Zn(S)_2L$ Complex. Pure ZnS nanocrystals (9.7 mg, 0.1 mmol), ligand L (58.5 mg, 0.1 mmol), and NaSCN (32.4 mg, 0.4 mmol) were first put into a Teflon-lined stainless steel autoclave with a 20 mL capacity, and then the autoclave was filled with ethanol up to 80% of the total volume. The autoclave was maintained at 130 °C for 24 h and then cooled to room temperature. The red single crystals of complex $Zn(S)_2L$ were obtained in 45% yield. Mp: turn brown at 218.5 °C. Anal. calcd: C, 68.94; H, 5.08; N, 7.84; S, 8.98. Found (%): C, 68.91; H, 5.12; N, 7.86; S, 8.96. IR (KBr pellet, cm^{-1}): υ(Zn−S), 474 (m). ^{1}H NMR (DMSO-d_6, 400 MHz, ppm) δ: 9.16 (s, 2H), 9.01 (d, J = 8.00 Hz, 2H), 8.87−8.70 (m, 3H), 8.49 (s, 1H), 8.39−8.34 (m, 3H), 8.20 (d, J = 8.00 Hz, 1H),7.94−7.82 (m, 5H), 7.72−7.62 (m, 3H), 7.51−7.42 (m, 2H), 7.25 (m, 1H), 4.42 (t, J = 7.20 Hz, 2H),1.80 (m, 2H),1.32−1.22 (m, 6H), 0.83 (t, J = 7.10 Hz, 3H). UV−vis (DMF): λ = 406 nm (excitation peak), 326 nm (higher excited state), 299 nm (the highest excited state). PL (DMF): 525 nm.

X-ray Crystal Structure Determination for $Zn(S)_2L$ Complex. The single-crystal diffraction data were collected on a Bruker Apex2 CCD diffractometer with Mo Kα radiation using the ω-scan mode (λ = 0.710 73 Å).[36] The structure was solved with direct methods using the Sir97 program and refined anisotropically with SHELXTL software using the full-matrix least-squares procedure.[37] All the nonhydrogen atoms were located from the trial structure and then refined anisotropically with SHELXTL, using the full-matrix least-squares procedure. The hydrogen atom positions were geometrically idealized and allowed to ride on their atoms and fixed displacement parameters. Data for $Zn(S)_2L$ were collected at T = 293 K. A small piece (0.38 × 0.30 × 0.16 mm^3) of a big cube crystal has been used for the data collection. $C_{41}H_{36}N_4S_2Zn$,

(35) (a) Cowley, A. R.; Davis, J.; Dilworth, J. R.; Donnelly, P. S.; Dobson, R.; Nightingale, A.; Peach, J. M.; Shore, B.; Kerr, D.; Seymour, L. *Chem. Commun.* **2005**, 845–847. (b) Pascu, S. I.; Waghorn, P. A.; Conry, T. D.; Betts, H. M.; Dilworth, J. R.; Churchill, G. C.; Pokrovska, T.; Christlieb, M.; Aigbirhio, F. I.; Warren, J. E. *Dalton Trans.* **2007**, 4988–4997. (c) Holland, J. P.; Aigbirhio, F. I.; Betts, H. M.; Bonnitcha, P. D.; Burke, P.; Christlieb, M.; Churchill, G. C.; Cowley, A. R.; Dilworth, J. R.; Donnelly, P. S.; Green, J. C.; Peach, J. M.; Vasudevan, S. R.; Warren, J. E. *Inorg. Chem.* **2007**, *46*, 465–485. (d) Pascu, S. I.; Waghorn, P. A.; Conry, T. D.; Lin, B.; Betts, H. M.; Dilworth, J. R.; Sim, R. B.; Churchill, G. C.; Aigbirhio, F. I.; Warren, J. E. *Dalton Trans.* **2008**, 2107–2110. (e) Holland, J. P.; Barnard, P. J.; Bayly, S. R.; Betts, H. M.; Churchill, G. C.; Dilworth, J. R.; Edge, R.; Green, J. C.; Hueting, R. *Eur. J. Inorg. Chem.* **2008**, 1985–1993.

(36) Bruker (2005), *APEX2 Software Suite (Version 2.0−2)*, Bruker AXS Inc., Madison, Wisconsin, USA.

(37) (a) Bruker (1997), *SHELXTL, Structure Determination Programs. Version 5.1*, Bruker AXS, Inc., Madison, Wisconsin, USA. (b) Farrugia, L. J. *J. Appl. Crystallogr.* **1999**, *32*, 837–838. (c) Sheldrick, G. M. (1997) *SHELX97, Programs for Crystal Structure Analysis (Release 97−2)*, University of Gotingen, Germany.

$M = 714.27$, monoclinic, space group $C2/c$, $a = 36.104(5)$ Å, $b = 11.621(5)$ Å, $c = 16.841(5)$ Å, $\beta = 97.646(5)°$, $V = 7003(4)$ Å^3, $Z = 8$, $Dc = 1.355$ g·mL^{-1}, $T = 293(2)$ K, μ(Mo Kα) = 0.856 mm^{-1}, 29 868 reflections measured ($1.84° \leq \theta \leq 27.63°$), 8118 unique [$I > 2\sigma(I)$], $R = 0.0618$, $wR_2 = 0.1977$. CIF files are available in the Supporting Information.

Quantum Chemical Calculations. Density functional theory (DFT) calculations were carried out using the Gaussian 03 suite of programs. The B3LYP functional was employed in conjunction with the all-electron 6-31G(d) basis set for all atoms.[38] Calculated molecular geometry obtained from X-ray diffraction crystallographic data.

Measurement of Single-Photon Excited Fluorescence (SPEF). The SPEF spectrum measurement of $Zn(S)_2L$ was performed on a HITACHI F-4500 fluorescence spectrophotometer at room temperature. The fluorescence quantum yield (Φ) is determined by using Coumarin 307 as the reference according to the literature method.[39] Fluorescence lifetime measurements were performed on a PicoQuant FluoTime 200 time-resolved fluorescence spectrometer by the time-correlated single-photon counting method (TCSPC) using a PDL 800-B picosecond diode Laser; a Hamamatsu R3809U-50 microchannel plate photomultiplier tube was used for detection. The decays were analyzed by "least-squares". The quality of the exponential fits was evaluated by the goodness of fit (χ^2).

Measurement of Two-Photon Excited Fluorescence and Two-Photon Absorption Cross Section of $Zn(S)_2L$. The two-photon absorption cross section (δ) was determined by using a femtosecond (fs) fluorescence measurement technique as described.[30,31] The two-photon excited fluorescence (TPEF) spectra were measured using a mode-locked Ti:sapphire laser (Coherent Mira900F) as the pump source with a pulse duration of 200 fs, a repetition rate of 76 MHz, and a single-scan streak camera (Hamamastu Model C5680-01) together with a monochromator as the recorder. The sample was dissolved in different solvents at a concentration of 1.0×10^{-3} mol L^{-1}. Fluorescein (pH = 11) in water was used as a reference, whose two-photon properties have been well characterized in the literature.[31] The intensities of TPEF spectra of the reference and the sample were determined at the same excitation wavelength. The two-photon absorption cross section was calculated by comparing their TPEF integral intensities, according to the following Equation:

$$\delta = \delta_{\mathrm{ref}} \frac{\Phi_{\mathrm{ref}}}{\Phi} \frac{c_{\mathrm{ref}}}{c} \frac{n_{\mathrm{ref}}}{n} \frac{F}{F_{\mathrm{ref}}}$$

Here, the subscripts ref stand for the reference molecule. δ is the TPA cross-sectional value, c is the concentration of the solution, n is the refractive index of the solution, F is the TPEF integral intensities of the solution emitted at the exciting wavelength, and Φ is the fluorescence quantum yield. The δ_{ref} value of reference was taken from the literature.[31]

Cell Culture and Staining. HeLa cells were passed and plated on a 35-mm cell culture dish with a coverslip and cultured in Dulbecco's Modified Eagle Medium (DMEM) (Gibco) supplemented with 10% fetal bovine serum (Sigma), penicillin (100 μg mL^{-1}), and streptomycin (100 ug mL^{-1}) at 37 °C in a humidified atmosphere with 5% CO_2 and 95% air for 24 h prior to staining. Immediately before labeling, cells were washed with PBS (phosphate buffered saline, pH = 7.2, Gibco) 3 times to remove the growth medium, and then 4 μL of the $Zn(S)_2L$ complex in DMSO (0. One mM) and 196 μL of PBS were added into the dish. After 30 min of incubation at 37 °C, 5% CO_2, the cells were washed with PBS (63) to remove unlabeled molecules, and then the cells were taken to a two-photon microscope for imaging.

Laser Scanning Confocal Microscopy Two-Photon Microscopic Imaging. A Zeiss LSM510 two-photon microscope equipped with a 63× or 100× oil-immersion objective was used to obtain bright field transmission and two-photon images. The excitation light was provided by a mode-locked Ti:sapphire laser (Mai Tai, Spectra-Physics Inc., USA) tuned to 800 nm, and a broadband-pass filter (480−600 nm) was used as emission filter. The microscope stage was outfitted with a CTI-3700 incubator, which maintained samples at 37 °C and 5% CO_2.

Cytotoxicity Assays in Cells. To ascertain the cytotoxic effect of $Zn(S)_2L$ treatment over a 24-h period, the MTT assay was performed. HeLa cells were passed and plated to 70% confluence in 96-well plates 24 h before treatment. Prior to $Zn(S)_2L$ treatment, the DMEM was removed and replaced with fresh DMEM, and then aliquots of $Zn(S)_2L$ stock solutions (500 μM in DMSO) were added to obtain final concentrations of 2, 5, 10, and 20 μM. The treated cells were incubated for 24 h at 37 °C and under 5% CO_2. Subsequently, the cells were treated with 5 mg/mL MTT (40 μL/well) and incubated for an additional 4 h (37 °C, 5% CO_2). Then DMEM was removed, the cells were dissolved in DMSO (150 μL/well), and the absorbance at 570 nm was recorded. The cell viability (%) was calculated according to the following equation: Cell viability % = $OD_{570(\mathrm{sample})}/OD_{570(\mathrm{control})} \times 100$, where $OD_{570(\mathrm{sample})}$ represents the optical density of the wells treated with various concentration of $Zn(S)_2L$ and $OD_{570(\mathrm{control})}$ represents that of the wells treated with DMEM+10% FCS. Three independent trials were conducted, and the averages and standard deviations are reported. The reported percent cell survival values are relative to untreated control cells.

Acknowledgment. This work was supported by National Natural Science Foundation of China (50532030, 20771001, 50703001, 20875001) and Scientific Innovation Team Foundation of Anhui Province (2006KJ007TD). We thank Prof. W.-T. Yu (Institute of Crystal Materials, Shandong University) for single-crystal data collection and structure solution. We thank Dr. Xuanjun Zhang, Dr. Lin Li, Prof. Zhonglin Lu, and Prof. Zhi Zheng for helpful discussions.

Supporting Information Available: The synthesis of ligand L; X-ray crystal structure determination for L; XRD pattern of ZnS nanocrystals, Figure S2; crystal packing of $Zn(S)_2L$ complex, Figure S3; IR spectra of pure L and complex $Zn(S)_2L$, Figure S4; the fluorescence lifetime measurement of $Zn(S)_2L$, Figure S5; X-ray crystallographic information files (CIFs) for $Zn(S)_2L$ and L. This material is available free of charge via the Internet at http://pubs.acs.org.

JA808606D

(38) GAUSSIAN98 References in http://www.gaussian.com.
(39) Demas, J. N.; Crosby, G. A. *J. Phys. Chem.* **1971**, *75*, 991–1024.